

High Speed Nonlinear Interferometric Vibrational Analysis of Lipids by Spectral Decomposition

Praveen D. Chowdary,^{†,‡} Vladimir A. Benalcazar,[†] Zhi Jiang,[†] Daniel M. Marks,[†] Stephen A. Boppart,^{*,†,§} and Martin Gruebele^{*,†,‡,||}

Beckman Institute for Advanced Science and Technology, Department of Chemistry, Department of Electrical and Computer Engineering, and Department of Physics and Center for Biophysics and Computational Biology, University of Illinois at Urbana-Champaign, Urbana, Illinois 61801

Unlike other CARS-based (coherent anti-Stokes Raman scattering) spectroscopy techniques, nonlinear interferometric vibrational spectroscopy (NIVS) is linear in analyte concentration and has a Raman line shape free of non-resonant background distortions. We use spontaneous Raman scattering as a high accuracy benchmark for NIVS. As a challenging comparison, we examine spectra in the CH stretching region of six lipid samples. Singular value decomposition and reference to an independent chemical assay are used to directly compare NIVS and spontaneous Raman scattering. We demonstrate that NIVS can determine the relative degree of unsaturation in six different lipid samples as accurately as spontaneous Raman spectroscopy, but 200 times faster. A skin tissue sample is mapped out to demonstrate quantitative lipid–protein differentiation with spatial resolution.

Spontaneous Raman spectroscopy is a convenient method for measuring vibrational spectra with well-defined line shapes and a linear dependence on sample concentration. Visible/NIR excitation allows penetration through many common solvents to access analytes. Thus Raman spectroscopy is a useful quantitative analytical tool. The drawback of spontaneous Raman spectroscopy is the low signal level and long averaging time required to obtain satisfactory signals.

Nonlinear Raman spectroscopies, such as coherent anti-Stokes Raman scattering (CARS),¹ offer much greater sensitivity by substituting a stimulated process for a spontaneous process. A sequence of pump-Stokes-pump pulses produces an anti-Stokes output pulse whenever a vibrational frequency Ω is in resonance (Figure 1 inset). Classical CARS used picosecond narrow bandwidth lasers for both the pump and Stokes pulses,¹ producing good spectral resolution but requiring spectral scanning to cover the spectrum. In 2002, Chen and co-workers,² Xie and co-workers,³ and Muller and co-workers⁴ reported multiplex CARS (mCARS), which uses a broadband Stokes pulse so CARS spectra can be

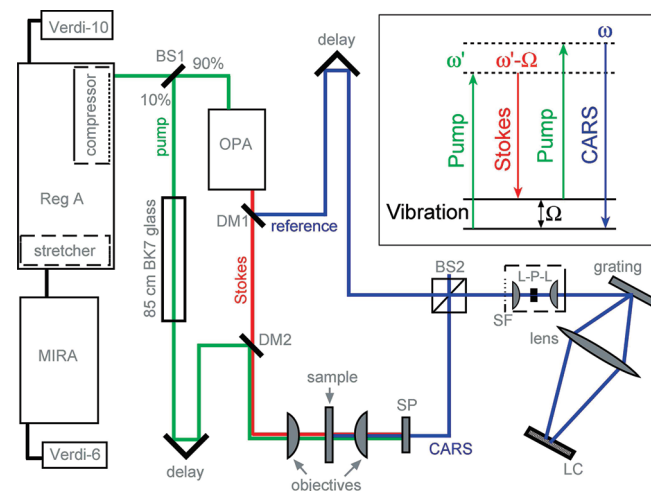


Figure 1. NIVS experimental layout. The Ti:Sapphire oscillator output (MIRA at 82 MHz, 25 nm fwhm at 807 nm, 380 mW) seeds the regenerative amplifier, which produces microjoule pulses (250 kHz, 1.1 W). 10% of this output, stretched to ~ 6 ps by passing through BK7 glass, serves as the pump. The remaining 90% pumps an OPA, which generates the Stokes (idler 30 nm FWHM at 1060 nm) and the reference (signal 25 nm FWHM at 855 nm). A microscope objective focuses the pump and Stokes collinearly onto the sample. The generated CARS signal is spectrally filtered (SP) and mixed with the reference at a 50:50 beamsplitter (BS2). The mixed beams are spatially filtered (SF) with a lens–pinhole ($30 \mu\text{m}$)–lens arrangement, and dispersed by a 1200 grooves/mm grating. The spectral interferogram is acquired on a line camera (2048 pixels). The pump-Stokes delay determines the instantaneous pump wavelength (typically 810 nm). DM1, DM2 = dichroic mirrors. BS1 = beamsplitter. The reference-CARS delay temporally separates the DC and phase-sensitive components of the interferogram. It is also the key for retrieving the complex analytical field from the real interferogram.

dispersed onto a detector array, parallelizing data collection. In 2004, Saykally and co-workers⁵ replaced the narrowband pump pulse by a chirped broadband pulse, maintaining high resolution while simplifying pulse generation to a single fs laser source.

The major drawback of these CARS techniques is that they measure only the output intensity $|E_{\text{CARS}}|^2 \approx |\chi^{(3)}|^2$. The conse-

- (2) Chen, P. C.; Joyner, C. C.; Patrick, S. T.; Benton, K. F. *Anal. Chem.* 2002, 74, 1618–1623.
- (3) Cheng, J. X.; Volkmer, A.; Book, L. D.; Xie, X. S. *J. Phys. Chem. B* 2002, 106, 8493–8498.
- (4) Muller, M.; Schins, J. M. *J. Phys. Chem. B* 2002, 106, 3715–3723.
- (5) Knutson, K. P.; Johnson, J. C.; Miller, A. E.; Petersen, P. B.; Saykally, R. J. *Chem. Phys. Lett.* 2004, 387, 436–441.

* To whom correspondence should be addressed.

† Beckman Institute for Advanced Science and Technology.

‡ Department of Chemistry

§ Departments of Electrical and Computer Engineering, Bioengineering, and Medicine.

|| Department of Physics and Center for Biophysics and Computational Biology.

(1) Shen, Y. R. *Principles of Nonlinear Optics*; Wiley Interscience: New York, 1984.

Table 1. Iodine Assay Gives the Number of C=C bonds per Milliliters of Oil ($N_{C=C}/mL$), Which Are Used to Calculate the Average Number of C=C Bonds Per Fatty Acid ($N_{C=C}/FA$) in the Oil^a

veg. oil	$N_{C=C}/mL$	I_2 assay $\times 1.44 \times 10^{21}$	saturated	oleic 1(C=C)	linoleic 2(C=C)	α -linoleic 3(C=C)	$N_{C=C}/FA$ calcd	$N_{C=C}/FA$ I_2 assay
coconut	0.18		91	6	2		0.10	0.11
olive	1.00		16	71	10	1	0.91	0.76
safflower	1.04		7	78	15		1.08	0.80
peanut	1.23		13	48	32		1.12	0.95
corn	1.89		13	28	58	1	1.47	1.43
soybean	1.92		15	24	54	7	1.53	1.45

^a Also shown are the approximate % compositions of saturated and unsaturated fatty acids in the different oils. The values of $N_{C=C}/FA$ calculated from the % fatty acid compositions is given for comparison.

quences are 2-fold: the signal depends quadratically on the amount of sample, and the line shape is distorted by nonresonant background in a difficult-to-control manner.⁶ As a result, CARS intensity-based techniques have been very useful for imaging general molecular content (e.g., lipid content in tissues, membranes or medical samples)^{7–10} but not for quantitative analysis (e.g., capable of distinguishing small differences between different lipids).

The nonresonant background and linearity problems were solved in 2004 by Boppart and co-workers with the introduction of nonlinear interferometric vibrational spectroscopy (NIVS), and its related imaging technique, nonlinear interferometric vibrational imaging (NIVI).¹¹ Like chirped CARS, NIVS uses a femtosecond Stokes pulse to provide broadband spectral coverage and pulse chirping to derive all pulses from a single femtosecond source, while maintaining high resolution. The key to NIVS is the addition of a reference pulse (also obtained from the same femtosecond source), which interacts with the CARS pulse in an interferometer to yield a signal linearly proportional to $\chi^{(3)}$.¹¹ NIVS measures both the real and imaginary components of the susceptibility independently, instead of just measuring its overall magnitude-squared. The NIVS signal is thus linear in concentration and has the simple Raman line shape suitable for quantitative analysis of mixtures or subtle spectral differences between compounds.

Here we directly compare NIVS with spontaneous Raman spectroscopy as the “gold standard” by obtaining spectra of six different oil samples with varying degrees of unsaturation. Quantitative decomposition of the NIVS and Raman spectra by singular value decomposition, and calibration with unsaturation data obtained independently by chemical titration of the oil samples, show that NIVS has the same ability as spontaneous Raman spectroscopy to distinguish subtle vibrational spectral features and determine relative degree of unsaturation. NIVS achieves the required signal-to-noise in less than 100 ms, which is over 200 times faster than Raman spectroscopy on a state-of-the-art Raman microscope. NIVS could thus be suitable for high-throughput applications where rapid and accurate spectral

measurements and a quantitative determination of sample content are required. We also map protein and lipid content in a skin sample to demonstrate a spectroscopic imaging application.

EXPERIMENTAL AND COMPUTATIONAL SECTION

Oil Samples and Chemical Assay. Six commercially available vegetable oils (coconut, olive, safflower, peanut, corn, soybean) with varying proportions of saturated and unsaturated fatty acids were studied (Table 1). The degree of unsaturation was measured by an iodine addition assay to provide data independent of the Raman and NIVS spectroscopies. For each assay, $V_{oil} = 0.250$ mL of oil was dissolved in 20.0 mL of chloroform. A 25.0 mL volume of Hanus solution (iodine bromide in glacial acetic acid, Sigma-Aldrich) was then added and kept in the dark for an hour. IBr is consumed by the C=C double bonds of the unsaturated fatty acids in this reaction. Then, 20.0 mL of 10% KI was added to convert excess IBr into I_2 , which was titrated against 0.1 M sodium thiosulfate. A 1 mL of 0.1 M sodium thiosulfate is equivalent to 0.05 mmol of I_2 . By subtracting the titrant volume V_T from the volume V_{blank} of a blank chloroform sample, the number of moles of IBr consumed by the C=C bonds in the oil is calculated. The number of C=C bonds per milliliters of the oil is obtained using

$$N_{C=C}/mL = \frac{(V_{blank} - V_T) \times 0.00005N_A}{V_{oil}} \quad (1)$$

where N_A is the Avogadro’s number. We also used the measured density and the average molecular weight of each oil (based on standard fatty acid compositions)¹² to obtain the average number of C=C bonds per fatty acid in the oil.

Raman Spectroscopy. The Raman spectra of the oils were acquired on a commercial confocal Raman microscope (Senterra, Bruker) using 532 nm excitation at 10 mW and an exposure time of 20 s per complete spectrum. Sample films were sandwiched between a slide and coverslip separated by a 125 μ m thick spacer. The Raman signal was collected in a back scattering geometry using an objective with a focal volume of ~ 2 μ m in the lateral and ~ 6 μ m in the axial directions. Spectral processing involved the correction for detector spectral sensitivity, removal of cosmic ray spikes, and baseline subtraction by polynomial fitting.

Nonlinear Interferometric Vibrational Spectroscopy (NIVS). The detailed theory of CARS and NIVS is discussed in the literature.^{13–16} For analytical purposes, NIVS differs from CARS

- (6) Evans, C. L.; Xie, X. S. *Ann. Rev. Anal. Chem.* **2008**, *1*, 883–909.
- (7) Wang, H. W.; Fu, Y.; Huff, T. B.; Le, T. T.; Wang, H. F.; Cheng, J. X. *Vibr. Spectrosc.* **2009**, *50*, 160–167.
- (8) Le, T. T.; Huff, T. B.; Cheng, J. X. *BMC Cancer* **2009**, *9*.
- (9) Rinia, H. A.; Bonn, M.; Muller, M.; Virtanen, E. M. *ChemPhysChem* **2007**, *8*, 279–287.
- (10) Windbergs, M.; Jurna, M.; Offerhaus, H. L.; Herek, J. L.; Kleinebudde, P.; Strachan, C. J. *Anal. Chem.* **2009**, *81*, 2085–2091.
- (11) Jones, G. W.; Marks, D. L.; Vinegoni, C.; Boppart, S. A. *Opt. Lett.* **2006**, *31*, 1543–1545.

- (12) Hilditch, T. P. *Br. J. Nutr.* **1949**, *3*, 347–354.

in two key aspects: it produces an output signal that is linearly proportional to the amount of sample, and interferometric phase reconstruction leads to reproducible lineshapes identical to spontaneous Raman lineshapes. We discuss these aspects and our instrumentation in more detail here.

For a Raman pump field envelope $E_P(\omega)$ and Stokes field envelope $E_S(\omega)$ (Figure 1 inset), the generated CARS output field is given by^{11,14}

$$E_{\text{CARS}}(\omega) \propto \int_0^{\infty} [\chi^{(3)}(\Omega)^* \int_0^{\infty} E_P(\omega')^* E_S(\omega' - \Omega) d\omega'] \times E_P(\omega - \Omega)^* d\Omega \quad (2)$$

$\chi^{(3)}(\Omega)$ is the third order susceptibility of the substance studied at vibrational frequency Ω . The term in brackets is the vibrational coherence created in the analyte by the pump and Stokes fields. Good spectral coverage requires a broadband Stokes field, and good spectral resolution usually entails the use of a narrowband pump field. If the ultrashort Stokes field is approximated by a delta function that gates the pump field at $t = 0$ when $\omega' = \omega_0$, the vibrational coherence simplifies to

$$\chi^{(3)}(\Omega)^* E_P(\omega_0)^* E_S(\omega_0 - \Omega) \quad (3)$$

If in addition the temporal envelope $E_P(t)$ of the pump field in eq 3 is constant, while the vibrational coherence decays (i.e., $E_P(t) \approx |E_P| \exp(-i\omega_0 t)$), eq 2 reduces to

$$E_{\text{CARS}}(\omega_0 + \Omega) \propto \chi^{(3)}(\Omega)^* E_P(\omega_0)^* E_S(\omega_0 - \Omega) |E_P| \propto \chi^{(3)}(\Omega)^* E_S(\omega_0 - \Omega) \quad (4)$$

The two conditions required for eq 4 to hold can be satisfied as discussed in the instrumentation subsection.

Experiments usually detect the CARS intensity $|E_{\text{CARS}}(\omega)|^2$, but this produces a distorted line shape from off-resonant contributions to the signal, as well as a quadratic concentration dependence. A signal with a Raman line shape (imaginary $\chi^{(3)}$) and a linear concentration dependence can be obtained if both the CARS amplitude and phase are extracted from the CARS output field by Fourier transform spectral interferometry,¹⁷ resulting in nonlinear interferometric vibrational spectroscopy (NIVS).

NIVS works by reconstructing the full complex CARS field from a real-valued spectral interferogram. To create the interferogram, the CARS output field $E_{\text{CARS}}(\omega)$ is mixed with a transform limited reference pulse E_{ref} in a Mach-Zehnder interferometer (Figure 1). The resulting spectral interferogram $I(\omega)$ (Figure 2A) contains DC components from the CARS and reference fields and the phase-sensitive cross term that will yield the NIVS signal

$$I(\omega) = |E_{\text{CARS}}|^2 + |E_{\text{ref}}|^2 + 2\text{Re}(E_{\text{CARS}} E_{\text{ref}}^* \exp(-i\omega t)) \quad (5)$$

- (13) Oron, D.; Dudovich, N.; Silberberg, Y. *Phys. Rev. Lett.* **2002**, 89.
- (14) Marks, D. L.; Boppart, S. A. *Phys. Rev. Lett.* **2004**, 92.
- (15) Knutson, K. P.; Messer, B. M.; Onorato, R. M.; Saykally, R. J. *J. Phys. Chem. B* **2006**, 110, 5854–5864.
- (16) Cheng, J. X.; Xie, X. S. *J. Phys. Chem. B* **2004**, 108, 827–840.
- (17) Lepetit, L.; Cheriaux, G.; Joffre, M. *J. Opt. Soc. Am. B* **1995**, 12, 2467–2474.

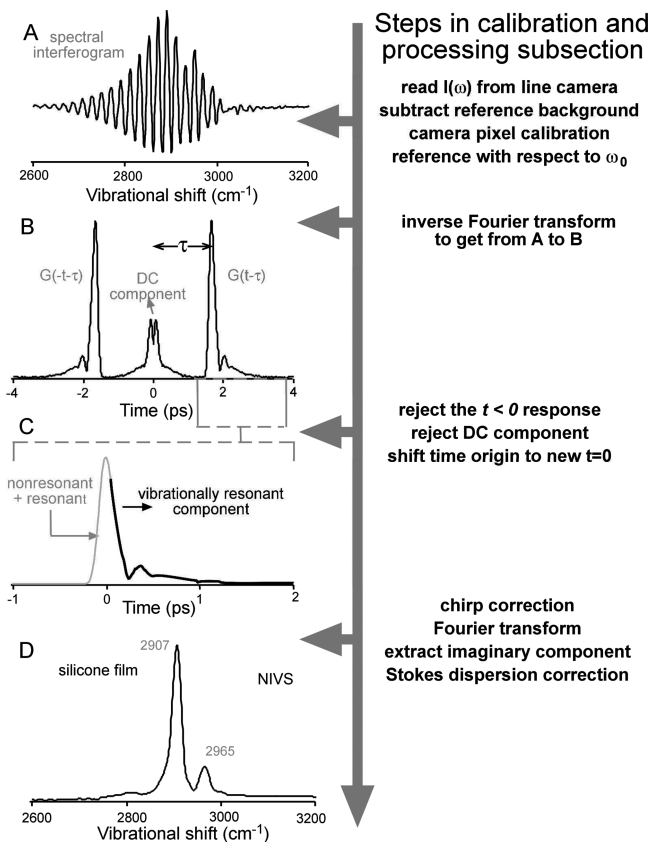


Figure 2. Working principle of Fourier transform spectral interferometry is demonstrated by extracting the NIVS spectrum of a silicone film starting from the interferogram acquired on the line camera. (A) Wavelength calibrated spectral interferogram referenced to the pump wavelength. The reference power spectrum is subtracted. (B) Modulus of the time domain polarization obtained by inverse Fourier transforming the interferogram in A. (C) The $t > 0$ response, identifying the short-time nonresonant (follows the Stokes pulse shape) and long-time resonant (vibrational dephasing) components. The temporal chirp of the pump can be corrected here. (D) NIVS spectrum of a silicone film obtained as the imaginary part by Fourier transforming the time response in C, and after the Stokes dispersion is corrected.

τ is the time delay between the CARS and reference pulses, essential for the reconstruction of the complex CARS field. The $|E_{\text{ref}}|^2$ term can be rejected by background subtraction of the known reference pulse. τ permits the rejection of the $|E_{\text{CARS}}|^2$ term by temporally separating the DC and phase sensitive components as follows. Letting $\chi(\omega) \equiv E_{\text{CARS}}(\omega) E_{\text{ref}}^*(\omega)$, we can express the inverse Fourier transform of eq 5 as (Figure 2B)

$$\text{FT}^{-1}(I(\omega)) = \text{FT}^{-1}(\text{DC}) + \chi(t - \tau) + \chi(-t - \tau) \quad (6)$$

The first term is a slowly varying DC component symmetric about $t = 0$ while the last two terms are time reversed from each other (eq 5 is real). Because of causality, there is no signal prior to the Stokes pulse initiating vibrational coherence. After the time origin is shifted to be the center of the Stokes pulse (Figure 2C), one can impose $\chi(t) = 0$ for $t < -T$, where T is greater than the Stokes pulse width. If the delay τ of the Mach-Zehnder interferometer is chosen larger than T , the two time-reversed terms in eq 6 do not overlap with each other or with the DC component (Figure 2B). The function $\chi(t - \tau)$ thus obtained by shifting and truncation is Fourier-transformed to recover $\chi(\omega) \propto \chi^{(3)}(\Omega)^* E_S(\omega)$

$-\Omega)E_{\text{ref}}(\omega)^*$. Both $\chi(\omega)$ and $\chi^{(3)}(\Omega)$ are linear in analyte concentration, but $\chi(\omega)$ is weighted by the known field envelopes E_S and E_{ref} .

In the absence of electronic resonances at ω , the nonresonant CARS background is real and can be rejected by discarding the real part of χ or $\chi^{(3)}$. The NIV spectrum is given by the imaginary part and matches the Raman spectrum, except for Raman depolarization effects.

Instrumentation. The use of narrowband pump and broadband Stokes pulses is typically required to attain good spectral resolution and broad spectral range simultaneously. However, NIVS achieves this by deriving the pump and Stokes pulses from the same ultrafast broadband source (figure 1), but chirping the pump pulse so $\omega' = \omega_0 + bt$ in eq 2. The spectral components of $E_P(\omega')$ are spread out in time, and time-gating by the ultrashort Stokes pulse at $t = 0$ ensures that only E_P with $\omega' = \omega_0$ contributes to the generation of vibrational coherence, thus retaining the narrowband spectral resolution.^{11,15} The chirp of the pump pulse causes a chirp of the CARS output field in eq 4, which must be computationally removed (steps C to D in Figure 2). The chirped pump field is described mathematically as

$$E_P(t) = |E_P| \exp(-at^2 - i\omega_0 t - ibt^2) \quad (7)$$

in the time domain.¹⁸ The constant a determines the Gaussian pulse envelope and b determines the chirp rate. Multiplying eq 4 by the conjugate phase factor e^{+ibt^2} removes the chirp in the CARS field and restores one-to-one correspondence between the anti-Stokes and vibrational frequencies. As discussed above eq 4, a must be small enough so $|E_P(t)|$ remains nearly constant while the vibrational coherence decays.

Figure 1 shows a schematic of our NIVS experimental setup, which is based on a 250 kHz regeneratively amplified oscillator. A modelocked Ti:Sapphire laser (MIRA, 82 MHz) seeds the regenerative amplifier (Coherent, RegA-9000, 250 kHz) which produces microjoule pulses. 10% of this output was used as the Raman pump, and linearly chirped to ~ 6 ps by passing it through an 85 cm block of BK7 glass. The remaining 90% of the output was used to pump an optical parametric amplifier (Coherent, OPA-9450), which produced the Stokes (idler) and reference (signal) pulses.

The pump and the Stokes fields were focused onto the sample by a microscopic objective filled to NA 0.3 (numerical aperture). A slide and coverslip with a 125 μm spacer identical to those used in the Raman experiment were used for direct comparison. The focal volume was $\sim 2 \mu\text{m}$ in lateral and $\sim 9 \mu\text{m}$ in axial directions. The nonlinear interaction of these fields with the sample generates the higher frequency CARS signal. The forward directed CARS signal was collected by an objective and was spectrally filtered from the pump, Stokes, and sample fluorescence, which all lie at longer wavelengths. The spectrally filtered CARS beam was then made collinear with the reference beam at a 50:50 cube beam-splitter. The CARS and the reference beams were spatially filtered at a pinhole to improve beam quality for robust interference. The mixed beams were then dispersed by a grating (1200 grooves/mm) to yield the spectral interferogram, which was recorded by a line camera (DALSA P2, 2048 pixels).

(18) Siegman, A. E. *Lasers*; University Science Books: New York, 1986.

The colors of the pump and Stokes pulses were tuned to target the C–H vibrational spectral range of 2800–3100 cm^{-1} . About 10 mW of pump and 1 mW of Stokes power were used, and the NIV spectra were acquired at a line rate of 1 kHz. The acquisition time for the NIV spectra reported here was 100 ms to achieve the same signal-to-noise ratio as the Raman spectrum (500:1 for the peak at 2857 cm^{-1} relative to the rms fluctuations of the baseline). We used 0.3 NA (numerical aperture) objectives for beam focusing and signal collection throughout. The pump, Stokes, and the reference fields were parallel-polarized.

Calibration and Processing. The CARS spectrum from a reference sample (acetone or silicone as in Figure 2) was monitored on a spectrometer (Ocean Optics QE65000), inline with the experimental setup, to calibrate the angular dispersion of wavelength on the line camera. The reference power spectrum was subtracted from the calibrated spectral interferogram to discard the bulk of the DC component. The wavelengths were then converted to Raman shifts by referencing to an approximate instantaneous pump frequency ω_0 (Figure 2A).

The interferogram was then inverse Fourier transformed to obtain the time domain polarization (Figure 2B). The residual DC and the negative time components were zeroed and the time origin was shifted to the peak of the CARS signal. The polarization then needed to be multiplied by the conjugate phase ibt^2 to correct for the pump-induced chirp. The chirp rate b was obtained by minimizing the width of the vibrational resonance of acetone at 2925 cm^{-1} . This procedure was iterated to optimize the values of ω_0 and b in such a way that the peak was observed at 2925 cm^{-1} with minimum width. The position and width of the 2907 cm^{-1} resonance of silicone can also be used for the same purpose.

The chirp-corrected polarization (Figure 2C) was then Fourier transformed to yield $\chi(\omega)$ (Figure 2D). The analysis presented in Results does not require field envelope normalization, which introduces additional noise. Rather than dividing $\chi(\omega)$ by E_S and E_{ref} to compare with the Raman line shape, we multiplied the Raman line shape by E_S and E_{ref} . Of course the NIVS signal-to-noise ratio decreases at the edges of the field envelopes, where less laser power was available to excite the sample.

The NIV spectrum must be corrected for the dispersion in the Stokes beam because of the transmissive optics in the beam path. This dispersion essentially leads to a linear scaling of the vibrational spectrum because of the interaction of the chirped pump frequencies (within the narrow bandwidth around ω_0) with the chirped Stokes frequencies (within the broad bandwidth). We used the silicone vibrational peaks at 2907 and 2965 cm^{-1} to correct for this scaling.

RESULTS

As an assay independent of Raman and NIVS, Table 1 lists the number of C=C bonds per milliliter ($N_{\text{C}=\text{C}}/\text{mL}$) in each oil obtained by iodine titration. Both NIVS and Raman data were calibrated against these absolute unsaturation values as detailed below. Table 1 also shows the average number of C=C bonds per fatty acid ($N_{\text{C}=\text{C}}/\text{FA}$) obtained by combining the iodine assay with a measurement of the oil densities and average molecular masses based on chain length distribution.¹² The measured $N_{\text{C}=\text{C}}/\text{FA}$ agrees with typical literature values based on fatty

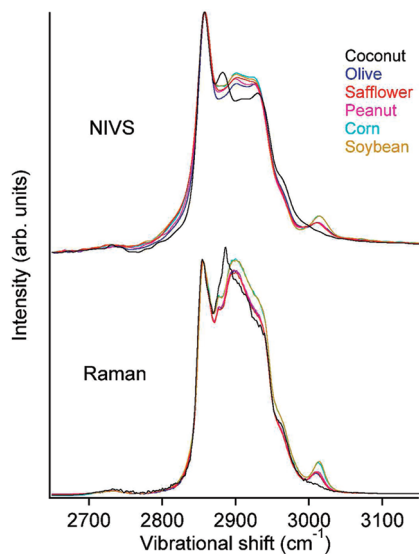


Figure 3. Comparison of polarized NIV and isotropic Raman spectra of various cooking oils. Relative intensity variations are expected due to the polarization sensitivity of NIVS and Raman depolarization ratios of different vibrational mode symmetries.

acid composition within the range of sample-to-sample variations expected of such oils.

Our main goal is to assess whether NIVS can determine the relative degree of unsaturation of different oils with the same relative accuracy as Raman spectroscopy. Using the setup shown in Figure 1, we obtained NIV spectra of six thin film samples of cooking oils (Table 1) in the challenging C–H stretching spectral range ($2730\text{--}3000\text{ cm}^{-1}$), where methyl, methylene, and $=\text{CH}-$ stretching bands overlap. The polarized CARS output field interfered with a reference field in a Mach–Zehnder interferometer, allowing reconstruction of the NIVS signal. NIVS has the same $\chi^{(3)}$ line shape as Raman spectroscopy and is linear in the analyte volume. For comparison, Raman spectra were acquired over the same spectral range on a Raman microscope. Quantitative results can be obtained by Raman spectroscopy in this spectral range, but not by chirped CARS, multiplex CARS, or similar techniques that detect only the anti-Stokes intensity, and thus suffer from nonresonant line shape distortion and a nonlinear dependence of the signal on the sample concentration.

Figure 3 compares the isotropic Raman and NIV spectra. For direct comparison with the NIVS signal, the Raman spectra were multiplied by the Stokes and reference field envelopes. All spectra were normalized to the same peak height at 2856 cm^{-1} . The C–H stretching spectral features of typical unsaturated fatty acids¹⁹ (listed in Table 2) in cooking oils are readily observed in the NIV spectra. For comparable signal-to-noise ratios (500:1), the NIV spectra were acquired 200 times faster than the Raman spectra: 100 ms versus 20 s.

The relative intensity variation of the two main peaks in the isotropic Raman and polarized NIV spectra is because of the inherent polarization sensitivity of NIVS. The linearly polarized reference field acts analogous to an analyzer in polarization-CARS

Table 2. Vibrational Peaks (in cm^{-1}) and Assignments of Unsaturated Fatty Acid Esters¹⁹

methyl oleate	methyl linoleate	methyl α -linoletae	vibrational assignments
3003	3012	3015	$=\text{C}-\text{H}$ stretch
2960	2951	2951	C–H stretch ($-\text{CH}_3$ asym)
2929	2924	2935	C–H stretch ($-\text{CH}_3$ sym)
2897	2903	2911	C–H stretch ($-\text{CH}_3$ sym)
2876	2877	2880	C–H stretch ($-\text{CH}_2$ asym)
2856	2855	2855	C–H stretch ($-\text{CH}_2$ sym)
2734	2732	2729	

experiments.^{3,20} Our reference field was polarized parallel to the pump and Stokes polarization, corresponding to an analyzer set for the polarized signal. Since the symmetric CH_2 stretching mode signal (2856 cm^{-1} , depolarization $\sim 1/5$) is better aligned with the reference than the asymmetric $\text{C}-\text{H}_2$ mode signal (2885 cm^{-1} , depolarization $\sim 3/4$),³ the peak at 2856 cm^{-1} appears relatively more intense than in the isotropic Raman spectra.

The intensity of the peak at 3010 cm^{-1} relative to the main saturated CH stretching peaks at 2856 and 2885 cm^{-1} represents the degree of unsaturation (number of $\text{C}=\text{C}$ double bonds) in the cooking oils (see Table 2). The Raman signal intensity of different oils in this region can be explained quantitatively by their relative degree of unsaturation. We want to assess whether NIVS can determine the degree of unsaturation as accurately as Raman spectroscopy.

To verify the quantifiable information content of the NIV spectra, we applied singular value decomposition (SVD)²¹ to the six NIV spectra and separately to the six Raman spectra. SVD is a linear decomposition technique and can be applied because both signals are linear in analyte volume. The purpose of SVD is to construct a set of orthonormal basis spectra $B_i(\Omega)$ such that each observed spectrum $S(\Omega)$ can be reconstructed exactly as

$$S(\Omega) = \sum_{i=1}^6 C_i B_i(\Omega) \quad (8)$$

with a different coefficient vector \mathbf{C} for each spectrum. Not all of the basis functions are correlated with the degree of unsaturation, and we can find an optimal parameter

$$U = \sum_i a_i C_i \quad (9)$$

to compare the predictions made by NIVS and Raman spectroscopy for the degree of relative unsaturation. Larger values of a_i weight the basis function B_i more.

Only two basis functions (B_2 and B_4) made a significant contribution to the unsaturated peak at 3010 cm^{-1} (Figure 4A). Figure 4B shows the coefficients C_2 and C_4 of the different oils obtained from NIVS. The linear combination $U = a_2 C_2 + a_4 C_4$ (dotted line in Figure 4B) best represents the degree of unsaturation from Table 1 ($N_{\text{C}=\text{C}}/\text{mL}$) was then obtained by least-squares fitting of the coefficients a_2 and a_4 . Since the NIV

(20) Cheng, J. X.; Book, L. D.; Xie, X. S. *Opt. Lett.* **2001**, *26*, 1341–1343.

(21) Press, W. H.; Teukolsky, S. A.; Vetterling, W. T.; Flannery, B. P. *Numerical Recipes: The Art of Scientific Computing*, 3rd ed.; Cambridge University Press: New York, 2007.

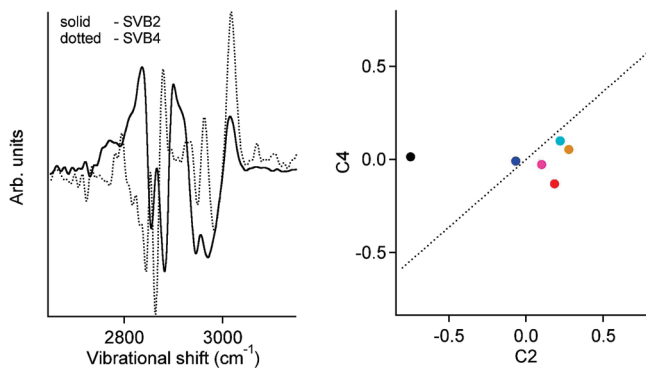


Figure 4. (Left) Singular value basis functions (SVBs) with significant contribution to the vibrational peak at 3010 cm^{-1} in the NIV spectra. (Right) The NIV spectral projections (C_2 along SVB2, C_4 along SVB4) of various oils in the 2D space of the SVBs. The dotted line is the appropriate linear combination of these SVBs that best represents the degree of unsaturation in the oils ($N_{\text{C}=\text{C}}/\text{mL}$). The color code for each oil is the same as in Figure 3.

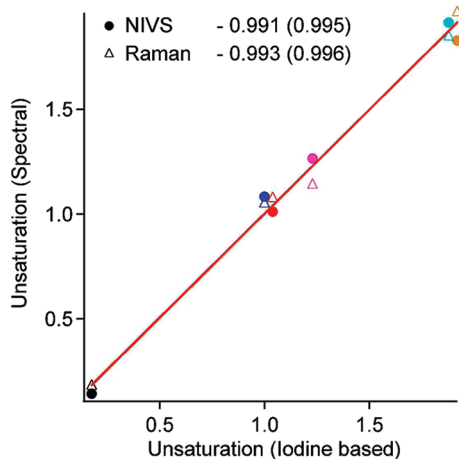


Figure 5. Relative $N_{\text{C}=\text{C}}/\text{mL}$ derived from NIV and Raman spectra plotted against $N_{\text{C}=\text{C}}/\text{mL}$ obtained from the iodine assay. Values shown are with respect to that of olive oil (1.44×10^{21}) as in Table 2. The slopes of the linear fits are listed with the correlation coefficients in parentheses. The color code for each oil is the same as in Figure 3.

spectra provide only the relative degree of unsaturation, we scaled U to match the absolute $N_{\text{C}=\text{C}}/\text{mL}$ obtained for olive oil from the iodine assay (Table 1).

The Raman spectra were subjected to the same analysis. Figure 5 shows a plot of both the NIVS (circles) and Raman (triangles) unsaturation $N_{\text{C}=\text{C}}/\text{mL}$ against that obtained from the iodine assay. Both spectroscopies produce excellent linear fits with slopes that are virtually identical. The linearity of the fits confirms the linear quantifiability of NIV spectra, which is as good as that of Raman spectra within the uncertainties of the iodine assay. The NIVS measurement is over 200 times faster than the spontaneous Raman measurement.

To demonstrate lipid/protein differentiation by NIVS in an image (NIVI), we scanned a $50\text{ }\mu\text{m}$ thick section of pig tissue at the dermis/subcutaneous fat layer boundary. Figure 6 shows the total resonant Raman signal in a $500 \times 500\text{ }\mu\text{m}$ sample ($<5\text{ }\mu\text{m}$ resolution), as well as NIVS spectral images color-coded by lipid content and protein content (as a fraction of maximum content observed), based on characteristic Raman peaks at 2855 and 2935 cm^{-1} .

DISCUSSION

Many CARS-related techniques have been developed to improve spectral fidelity and imaging capabilities. For example, frequency modulation CARS, heterodyne CARS, and interferometric CARS, use picosecond pulses good for imaging, but without the spectral range needed for chemometric analysis.^{6,16} To obtain broadband coverage, Xie and co-workers combined mCARS with polarization detection to suppress the nonresonant background better. This approach definitely improves the resonant vibrational contrast and is excellent for imaging of general lipid content.³ However, a residual background remains in the mCARS spectra when compared to the spontaneous Raman spectra,²² and the signal is not linear in population. In contrast, NIVS achieves complete background rejection, verified by comparison to Raman spectra, as well as quantifiable linearity (Figure 5). The use of polarization selection to reject background also applies to NIVS, as the nonresonant background has a depolarization of $1/3$ and polarization selection is inherent in the anti-Stokes-reference beam interaction with parallel polarization. Further optimization of the reference polarization could be useful for detecting weak transitions with various polarization ratios.

Computational tools have been developed to extract the Raman line shape from CARS intensities, such as the maximum entropy method.²³ These tools can greatly improve ordinary CARS lineshapes, but still have to make assumptions, such as the imaginary part of $\chi^{(3)}$ being much smaller than the off-resonant background, yet far removed from resonance. It is currently not clear how such procedures affect spectra when signal-to-noise ratios in excess of 100 are desired. Similar computational cleanup may turn out to be useful to improve the line shape further even on NIVS data.

Of the nonlinear Raman spectroscopy tools developed in the past decade, only femtosecond stimulated Raman scattering (FSRS)²⁴ can be compared with NIVS as an analytical tool. In FSRS, a white-light continuum provides broad spectral coverage, and a picosecond narrowband pump pulse achieves a reported spectral resolution of 10 cm^{-1} , comparable to the resolution reported here. The signal is linear in sample concentration. The subtraction required to produce Raman lineshapes from FSRS can create small negative artifacts, but the lineshapes are far superior to intensity-detected CARS lineshapes. A quantitative comparison of signal-to-noise ratios (S/N) is not possible, but for neat cyclohexane (similar density of CH_2 groups and Raman cross sections compared to neat oil) and a path length of 1 cm , S/N of $\sim 300:1$ were achieved in 100 ms (100 pulses).²⁴ This can be compared with a S/N of $500:1$ achieved by NIVS with a 0.0125 cm path length in 100 ms . Thus NIVS appears to perform better in that regard. The authors of ref 24 note that saturation of the S/N in FSRS should not occur if difference spectra are measured instead of the absolute spectra recorded there, and of course their technique has the advantage of very high time resolution when lower S/N is sufficient.

(22) Volkmer, A. *J. Phys. D* **2005**, *38*, R59–R81.

(23) Vartiainen, E. M.; Rinia, H. A.; Muller, M.; Bonn, M. *Opt. Express* **2006**, *14*, 3622–3630.

(24) McCamant, D. W.; Kukura, P.; Yoon, S.; Mathies, R. A. *Rev. Sci. Instrum.* **2004**, *75*, 4971–4980.

(25) Kraft, C.; Dietzek, B.; Popp, J. *Analyst* **2009**, *134*, 1046–1057.

(26) Freudiger, C. W.; Min, W.; Saar, B. G.; Lu, S.; Holtom, G. R.; He, C. W.; Tsai, J. C.; Kang, J. X.; Xie, X. S. *Science* **2008**, *322*, 1857–1861.

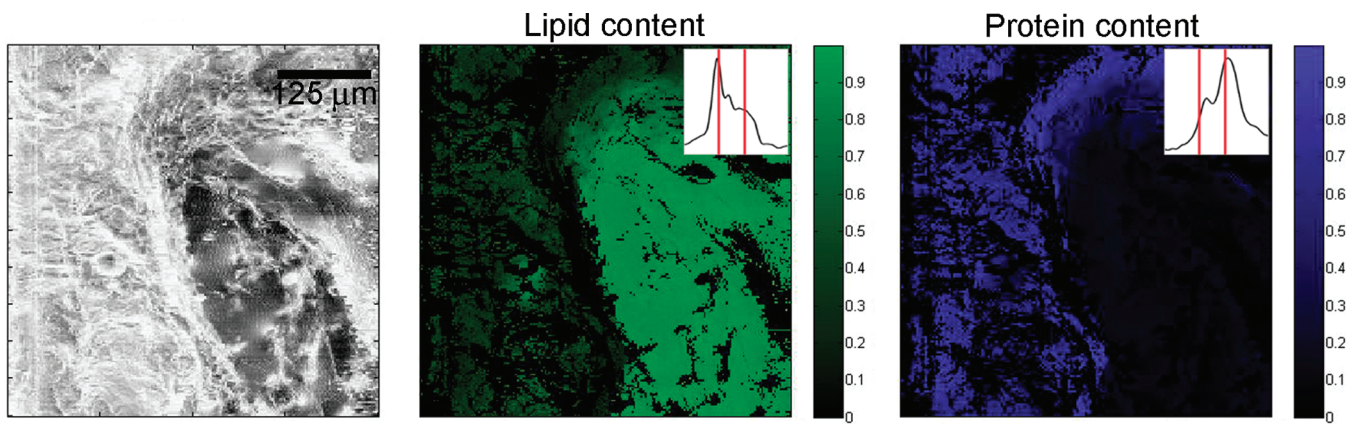


Figure 6. NIVS chemical imaging of an unstained skin section (interface between pig dermis and subcutaneous adipose tissue). Left: Total resonant power. Middle: Spatial map of lipid content (from black to green as fraction of maximum). Right: Spatial map of protein content (from black to blue as fraction of maximum). The section was $50\text{ }\mu\text{m}$ thick. The insets shows average NIVI spectra corresponding to the green and blue color-coded regions, with vertical red lines indicating 2855 cm^{-1} (CH_2) and 2935 cm^{-1} (CH_3) stretches.

NIVS-based imaging (NIVI) could be a useful tool for analytical imaging applications. For example, Krafft et al.²⁵ discuss the need for combining Raman spectroscopy spectral quality and CARS microscopy imaging for various bioanalytical and biomedical applications. They had to implement Raman spectroscopy and CARS microscopy separately. NIVS-based imaging combines the best of these two techniques, allowing fast imaging with spectral pixels that are linear in analyte concentration and have reproducible lineshapes. For lipid studies specifically, such quantification would be useful.^{7,8} Instead of just identifying lipids in tissues, spectral signatures of unsaturation, such as from omega-3 fatty acids, could be studied. There has been some interest in the effects of omega-3 fatty acids on cancer cell lipid metabolism.²⁶

Along the lines of the skin tissue scan shown in Figure 6, we recently developed chemometric imaging useful for the pathology of cancer tissue using intensity analysis of NIV imaging instead of the SVD analysis outlined here.²⁷ The underlying idea is that

carcinomas have a very different ratio of lipid to protein content, which can be readily quantified if accurate lineshapes can be measured. Adaptation of SVD-decomposed NIV imaging to cancer diagnosis could allow small (sub-0.1 mm) cancerous incursions to be identified in thin sections (<0.1 mm) of healthy tissue, judging from the S/N and high linearity of the signal obtained in our oil study presented here.

NIVS could be further improved by increasing its bandwidth, or by allowing the interferometry to be recorded in a single shot to increase time resolution. A number of schemes have been developed in these directions.^{28–30}

ACKNOWLEDGMENT

This work was supported by a grant from the National Institutes of Health, National Cancer Institute, R21/R33 CA115536 (S.B. and M.G.). Z.J. was supported by the Beckman Fellows Program. M.G. and P.C. were additionally supported by the James R. Eiszner Chair.

Received for review January 25, 2010. Accepted March 19, 2010.

AC100222C

- (27) Benalcazar, W. A.; Chowdary, P. D.; Jiang, Z.; Marks, D. L.; Chaney, E. J.; Gruebele, M.; Boppart, S. A. *IEEE J. Sel. Top. Quant. Elec.* **2010**, DOI: 10.1109/JSTQE.2009.2035537.
- (28) Lee, Y. J.; Cicerone, M. T. *Opt. Express* **2009**, *17*, 123–135.
- (29) Lim, S. H.; Caster, A. G.; Leone, S. R. *Opt. Lett.* **2007**, *32*, 1332–1334.
- (30) Kee, T. W.; Zhao, H. X.; Cicerone, M. T. *Opt. Express* **2006**, *14*, 3631–3640.